ADVANCED MATERIALS
www.advmat.de

www.MaterialsViews.com

Synthesis of Chemically Bonded Graphene/Carbon Nanotube Composites and their Application in Large Volumetric Capacitance Supercapacitors

Naeyoung Jung, Soongeun Kwon, Dongwook Lee, Dong-Myung Yoon, Young Min Park, Anass Benayad, Jae-Young Choi, and Jong Se Park*

Electrical double-layer capacitors (EDLCs) store electric charge at electrode/electrolyte interfaces. Because of the electrostatic mechanism that enables storage of charge at the interface, in order to store large amounts of charge, electrodes with high surface area and high conductivities are required. Usually, activated carbon (AC)-based electrodes with large surface areas (ca. 1000 m^2 g^{-1}) are the state-of-the-art electrodes used in EDLCs. However, despite the huge surface area, large portions of the micro/macropores present within the AC prove to be ineffective spaces for the adsorption of the electrolyte on the surface of the electrodes, which deteriorates the function of the EDLCs. To address this challenge, the use of graphene—a 2D material with a large surface area—has attracted tremendous interest because of the enormous surface area (ca. 2600 m^2 g^{-1}) and high electrical conductivity.[1–3]

Currently, significant research efforts have been directed toward creating porous graphene electrodes with a large electrolyte-accessible area.[4,5] However, the electrodes fabricated have possessed spacious voids and random stacking of graphene sheets; hence, the materials exhibited smaller volumetric capacitance than commercially available AC electrodes, despite the large gravimetric capacitance. In another approach to increase the capacitance, graphene composite structures containing other carbonaceous nanomaterials, such as carbon nanotubes (CNTs) and AC, were employed.[6–9] However, the restacking force between the graphene layers dispersed in a solution leads to agglomeration of the graphene layers, hampering the permeation of electrolyte between the layers.

In this report, we synthesized a graphene–CNT composite with lamellar structure by amidation reaction. Complementary bonding between the graphene oxide (GO) and CNTs prevented restacking between graphene layers and the agglomeration of CNTs. CNTs attached onto the edges and surface of the graphene not only act as spacers to increase the electrolyte-accessible surface area, but also provide a 3D electrical conduction path.[9] To the best of the authors' knowledge, we have demonstrated the largest volumetric capacitance (165 F cm^{-3}) ever shown by carbon-based electrodes by intercalating graphene sheets with individual CNTs without agglomeration. The graphene electrode did not contain any binder or additives and was extremely thin and flexible.

Chemically Bonded GO/CNT Composites: Specific cross-linking based on the reaction with *N*-hydroxysuccinimide ester (NHS ester) is commonly used for protein modification.[10] NHS chemistry has also been used to make hybrids of GO nanosheets and Fe_3O_4 nanoparticles.[11] The procedure for synthesizing amide-bonded GO/CNT hybrids is schematically illustrated in **Figure 1**. Amine-functionalized CNTs[12,13] reacted with NHS-activated GO (NHS-GO) in a weight ratio of 1:5.[11,12] To synthesize the GO-CNT composite, the CNTs were oxidized and amine groups were introduced on the CNT surfaces. Oxidized CNTs were noticeably well-dispersed in aqueous solution, while NH_2-CNTs showed discernibly decreased dispersibility. NH_2-CNTs, however, can be dispersed into water with high concentration without any agglomeration for about a day after tip sonication for a short time (40 s). After bonding the NH_2-CNTs to NHS-GO by amidation reaction, the [GO-CNT] composite was stable for more than several weeks without any agglomeration or chemical change.

An aqueous mixture of NHS-GO and NH_2-CNT before the amide bond formation was brownish in color and exhibited a ultraviolet-visible (UV-Vis) absorption peak at 201 nm, as shown in **Figure 2**a. After heating at 80 °C for an hour with stirring, the solution turned black and exhibited double peaks at 228 and 250 nm, corresponding to $\pi \rightarrow \pi^*$ transitions of aromatic C=C bonds developed in the UV-Vis spectra. The NHS-GO and NH_2-CNT were connected by an amide bond, which restored the broken sp^2 connections in GO and extended the conjugation between GO and CNT through the chemical link.[11,14] After the reaction, the pH was lowered to around 7 from 8 because of the liberation of NHS acid.

The formation of the amide bond was confirmed by Fourier transform infrared (FTIR) spectroscopy and X-ray photoelectron spectroscopy (XPS). Figure 2b shows the FTIR spectra of the [NHS-GO/NH2-CNT] mixture before reaction and that of the as-made amide bonded [GO-CNT] composites. After amidation, bands corresponding to C–N stretching (1215 cm^{-1}), amide C–N stretching(1477 cm^{-1}), amide N–H bending (1560 cm^{-1}),

Dr. N. Jung, S. Kwon, D.-M. Yoon,
Y. M. Park, J. S. Park
R&D Center
Samsung Corning Precision Materials Co.,
Ltd. Tanjeong-myeon
Asan-city, 336-725, Republic of Korea
E-mail : naeyoung.j@samsung.com
D. Lee, A. Benayad, J.-Y. Choi
Graphene Research Center
Samsung Advanced Institute of Technology
Yongin, 446-712, Republic of Korea

DOI: 10.1002/adma.201302788

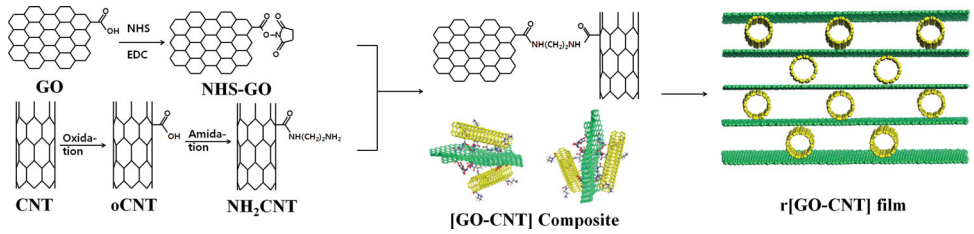

Figure 1. Synthesis scheme depicting the reaction between a GO layer and a CNT and a view of the fabricated r[GO-CNT] film. a) Reaction scheme representing the formation of the [GO-CNT] composite. The amine groups were introduced into the CNT after an oxidation reaction. The amine-functionalized CNTs reacted with NHS-activated GO, resulting in the [GO-CNT] composite. The filtration of the [GO-CNT] aqueous composite resulted in a lamellar r[GO-CNT] film.

and C–O stretching(1703 cm^{-1}) were observed,[11,12] as indicated by the arrows, along with peaks corresponding to the original C–O bond (1064 cm^{-1}) and C–OH bond (1358 cm^{-1}) of the GO.[15] The strong peak at 1630 cm^{-1} could be attributed to the presence of O–H groups on the surface of the GO/CNT composites arising from the tightly bound ambient atmospheric moisture or from crystal water associated with KBr used for the preparation of the IR spectroscopy specimens.[12]

High-resolution XPS also revealed the chemical bonding in the [GO-CNT] composite in comparison to that in GO (Figure 2 c–f). The peak areas and the use of the atomic sensitivity factors provided the atomic concentration of each element, providing a quantitative measure of the extent of functionalization. Besides the main C–C peak at 284.5 eV, additional photoemission at higher binding energies of 286.5 and 287.8 eV for the GO C1s indicated the presence of oxygen atoms bonded to carbon atoms as in –C–O and C=O, respectively.[1,16] The [GO-CNT] composites showed a peak at 285.9 eV, which can be ascribed to the C–N bond formation. The appearance of N 1s core level peak after the amidation reaction indicated nitrogen insertion. The oxygen concentration decreased from 33% to 26% after the amide bond formation process, while the concentration of N increased from an insignificant 0.5% to 5%, indicating the conversion of carboxylic acid group to amide, in tune with the FTIR spectroscopy results.

An aqueous solution of the stable [GO-CNT] composite was reduced to r[GO-CNT] by the microwave hydrothermal (MWHT) method with the aid of hydrazine and ammonia.[14,16–18] Transmission electron microscopy (TEM) showed the morphology and microstructure of the [GO-CNT] (Figure 2e and f). The selected area electron diffraction (SAED) patterns of [GO-CNT] and r[GO-CNT] clearly indicated that the graphene sheets were randomly overlapped and the 2D honeycomb crystal was maintained.[18–20] Based on high-resolution (HR)-TEM analysis of [GO-CNT], it can be seen that the CNTs were attached along the edge of the GO as well as on the basal plane of the GO. CNTs that bind on the graphene surface lay down horizontally on the graphene surface. Even after reduction, CNTs were strongly bound on the graphene edge and surface (see Figure S1 in the Supporting Information).

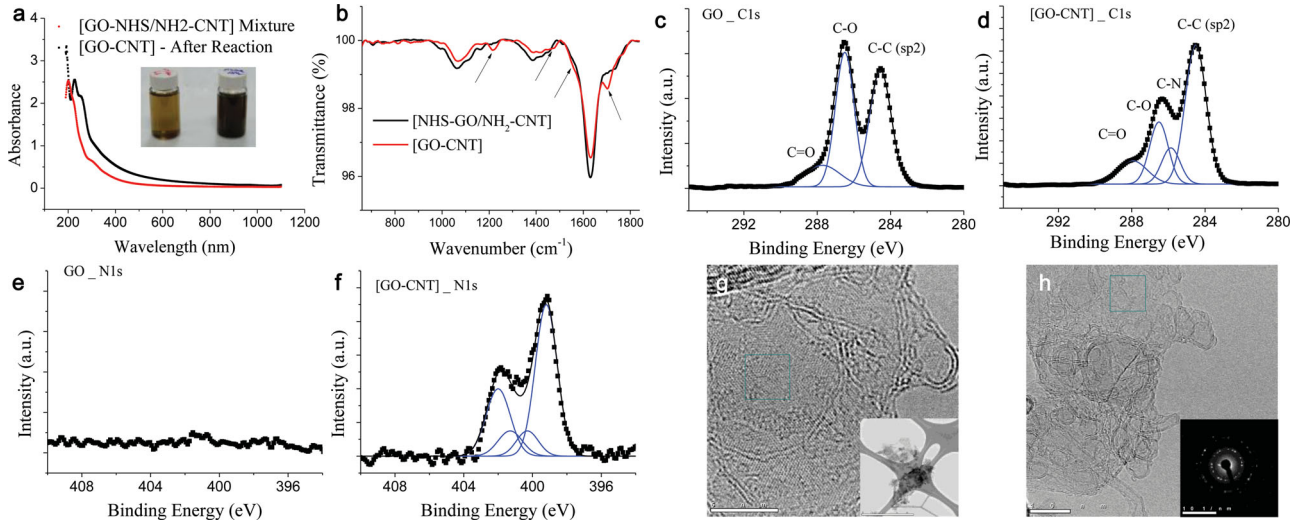

Figure 2. Characterization of the chemically bonded graphene-CNT composite. a) UV-vis absorption spectra of the [NHS-GO/NH_2-CNT] mixture and [GO-CNT] after the amidation reaction. The inset shows the color of the solution before and after the amidation reaction. b) FTIR spectra of [NHS-GO/NH_2-CNT] mixture and [GO-CNT] composite. c–f) C1s and N1s XPS spectra of GO and [GO-CNT]. g,h) TEM images of [GO-CNT] composites at different magnifications. The insets are a low magnification TEM image and SAED pattern, respectively

ADVANCED MATERIALS
www.advmat.de

www.MaterialsViews.com

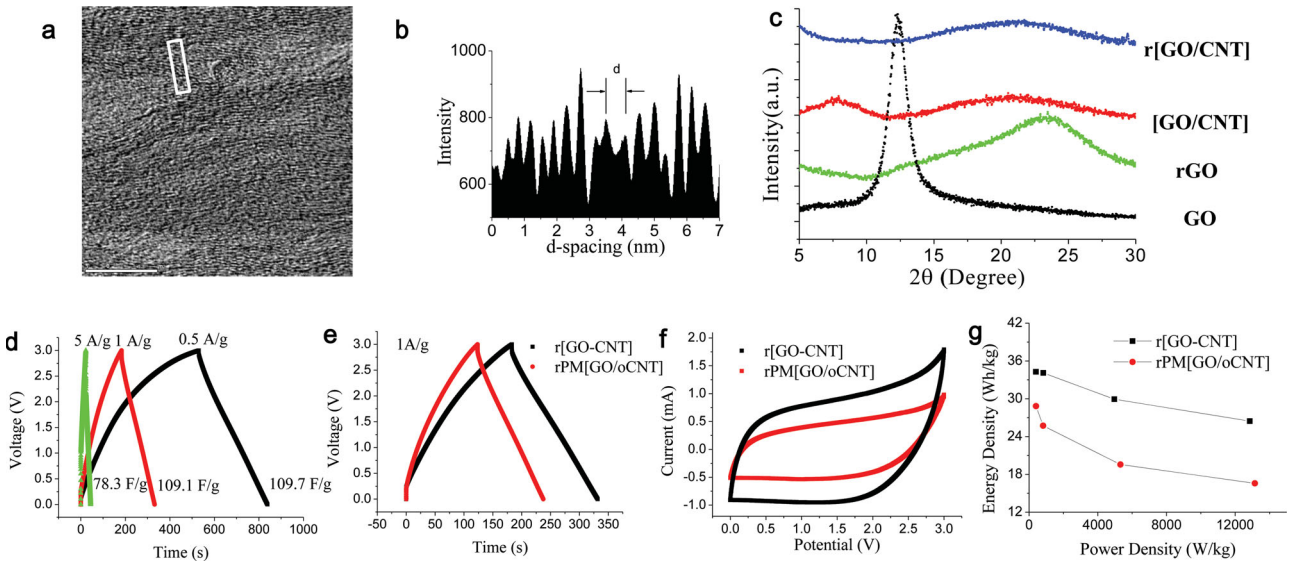

Figure 3. Lamellar structure and electrochemical performance of r[GO-CNT] and rPM[GO/oCNT] composites. a) TEM cross-section of the FIB cut r[GO-CNT] film. b) The cross-sectional profile of the portion enclosed in the white box in (a). c) XRD spectra of GO, rGO, [GO-CNT], and r[GO/CNT]. d) Galvanostatic charge and discharge curves of r[GO/CNT] at current densities of 5, 1, and 0.5 A g^{-1}. e) Galvanostatic charge and discharge curves of r[GO-CNT] and rPM[GO/oCNT]. f)C–V profiles of r[GO-CNT] and rPM[GO/oCNT]. g) Ragone plot of r[GO-CNT] and rPM[GO/oCNT].

Lamellar Structure: In order to achieve a highly dense structure, the reduced [GO-CNT] (r[GO-CNT]) lamellar structure film was fabricated using a flow-directed assembly. Also, the oxidized CNTs were simply mixed with an aqueous solution of GO, which was reduced to produce a reduced physically mixed (rPM) [GO/oCNT] film. Cross-sectional images of chemically bonded r[GO-CNT] were compared with rGO and physically mixed rPM[GO/oCNT] film (see Figure S2 in the Supporting Information) The thickness of the r[GO-CNT] composite electrode films obtained by filtration could be controlled from 1 μm to hundreds of μm by controlling the concentration and amount of the solution. The sheet resistance of the 5 μm thickness r[GO-CNT] electrode, measured with the four-point probe method, was 50 Ω per square. The scanning electron microscopy (SEM) images show a lamellar structures in the case of rGO, rPM[GO/oCNT], and r[GO-CNT] fragmented after immersion into liquid nitrogen, while rGO films showed the presence of nearly perfectly aligned rGO sheets that densely stacked and formed a graphite-like structure.[20] r[GO/oCNT] and rPM[GO/oCNT] films exhibited large void spaces of 100–200 nm between the graphene layers, indicated as white arrows(A6, see Figure S2 in the Supporting Information) , which is expected to be made by the sliding out of graphene layers from the graphene stacks during sample preparation. It is worth noting that the CNTs were dragged out from the graphene layered structure in rPM[GO/oCNT], while CNTs are not observed in the cross-section of r[GO-CNT] because of their chemical bonding to the graphene edge and surface. The void structure observed in the SEM cross-sectional image was absent in the sample prepared by focused ion bean transmission electron spectroscopy (FIB-TEM) (**Figure 3** a) because the voids were made during the SEM sample preparation procedure. The intensity profile of the HR-TEM image (Figure 3b) indicated that the *d*-spacing of the graphene layers varies in the range of 0.33 to 0.55 nm, which is larger than the average layer-to-layer spacing of 0.36 nm observed in the rGO film.[20] The inserted CNT may be expected to prevent close contact between the graphene layers, leading to an increase in the *d*-spacing between the graphene layers.

The graphene-to-graphene layer distance was also measured with X-ray diffraction (XRD; Figure 3c) The layer-by-layer stacked GO showed a strong peak centered at $2\theta = 12.36°$, corresponding to 7.1 Å, while the [GO/CNT] composite film showed two weak peaks centered at 7.7° and 19.5°, corresponding to 11.5 and 4.5 Å, respectively. Since CNT hampers close contact between the graphene basal planes, graphene layers were not well stacked and the sample showed a very weak XRD pattern with a stacking distance of 11.5 Å. After MWHT reduction, the sharp peak from graphene oxide disappeared and a broader peak centered at 23.3° (3.8 Å) appeared, suggesting deoxygenation of graphene oxide, resulting in shorter graphene interlayer spacing. Note that the peak position shown by r[GO/CNT] (20.9°), corresponding to an interlayer distance of 4.2 Å, was clearly shifted in comparison to the peak position shown by rGO, indicating that the chemically bonded CNTs were well intercalated between the graphene layers, acting as spacers.

Electrochemical Performance of the r[GO-CNT] Film Electrode: The electrochemical properties of chemically bonded r[GO/CNT] film were compared with those of the physically mixed rPM[GO/CNT] film. The difference between rPM[GO/oCNTs] and r[GO/CNT] is the existence of complementary cross-linking between the graphene layers and CNTs, which hampers restacking between graphene layers and agglomeration of CNTs during the film fabrication process.

To evaluate the supercapacitive performance of the r[GO-CNT] hybrid in comparison to that of the rPM[GO/oCNT], two electrode symmetric coin cells were assembled and organic 1 m tetraethyl ammonium tetrafluoroborate (TEABF4) in polycarbonate was used as the electrolyte. The organic electrolyte

operated at a wide voltage range, thus enabling the achievement of higher energy and power density even with lower specific capacitance, when compared to aqueous electrolyte solution.[4,6,21] The electrode loading level was varied between 150 and 500 μg per electrode (ca. 1.1 cm^2 × 1–3 μm). The electrochemical performance was analyzed through both galvanostatic charge/discharge profiles and cyclic voltammetry (CV).

Typical charge/discharge profiles of the r[GO-CNT] hybrid electrodes with different current densities are shown in Figure 3d. The slightly distorted triangular charge/discharge profiles ae similar to the typical shape shown by electrical double layer capacitors (EDLCs) with good performance. A small voltage drop across the capacitor system, which was caused by equivalent series resistance, was observed in the curve from 3.0 to 2.8 V. The specific capacitance, *C*, of the electrode was calculated using the slope of the discharge line according to the following equation:

$$C = It/m\Delta V \quad (1)$$

where *I* is the applied current, *m* is the mass of the active material, ΔV is the potential range (3 V), and *t* is the time to discharge. We measured the specific capacitance of the r[GO-CNT] electrode at three different current densities. The specific capacitance of the graphene composite electrode decreased from 110 to 78 F g^{-1} with an increase in the charge/discharge rate when the current density increased from 1 to 5 A g^{-1}. However, the specific capacitance remained unchanged between 0.5 and 1 A g^{-1}. The electrode structure perpendicular to the flow of electrons and ions limited the rate performance at high current densities. By developing crumpled, ball-like, or mechanically smashed composites, rate performances can be improved.[22]

Despite the intense focus of numerous reports on EDLCs electrodes on the gravimetric capacitance, the volumetric capacitance is a crucial factor determining the design and practical application of these electrodes. Based on the thickness measured by SEM, the volume of each electrode was calculated. The average density was calculated as 1.5 g cm^{-3}, which is almost 70% of that of graphite (2.1–2.3 g cm^{-3}). Hence, the volumetric capacitance of this composite was calculated as 165 F cm^{-3}, which is the highest value ever reported for carbon-based electrodes, to the best of our knowledge. The rPM[GO/oCNT]-based electrode, however, exhibited a capacitance of 82.7 F g^{-1} at 1 A g^{-1}, which was almost 30% lesser than r[GO-CNT]-based electrodes. This reduction can probably be ascribed to the less effective surface area of the graphene composites because of the inevitable restacking of graphene layers and agglomeration of CNTs. Furthermore, it can be also ascribed to the fact that the CNTs physically attached to graphene provide an effective conduction path.[9]

The r[GO-CNT] hybrid films showed straight triangular galvanostatic charge/discharge profiles and rectangular CV curves without any redox peaks, indicating ideal capacitive behavior. The pseudocapacitance effect, which can be enhanced by surface functional groups containing oxygen and nitrogen by additional Faradaic reaction, was not observed. It should be also noted that the CVs were still rectangular even at high scan rates of 0.2 V s^{-1}, indicating rapid charging and discharging with a low equivalent series resistance of the electrodes. This indicates the formation of an efficient electrical double layer and fast ion transport within the graphene composite electrodes. The integrated area of the CV curves shown by r[GO-CNT] was larger than that of rPM[GO/oCNT] within the potential window of 0 to 3 V, confirming the smaller capacitance of rPM[GO/oCNT]. In order to compare the overall performance of the r[GO-CNT] to that of the rPM[GO/oCNT] films, energy density and power density were calculated by the following equations:

$$E = 1/8 \times C(\Delta V)^2 \quad (2)$$

$$P = E/t \quad (3)$$

where *C* is the specific capacitance of the cell, ΔV is the potential range (3 V), *P* is the power density, and *t* is the time to discharge. The r[GO-CNT] composite films showed the best performance with a high energy density of 34.3 W h kg^{-1} at 400 W kg^{-1}, which gradually decreased to 26.5 W h kg^{-1} at 12.8 kW kg^{-1}. Meanwhile, the rPM[GO/oCNT] film showed less effective electrochemical energy and power densities.

Large Volumetric Capacitance: Generally, GO has carboxylic groups at its edges and epoxy and hydroxyl groups on the basal plane.[23] Since carboxylic groups act as the reaction site for the NHS activation, NHS activation can be expected to occur largely along the edge and marginally on the basal plane. Hence, the CNTs bind along the chemically reactive graphene edge and a relatively small amount of CNTs bind on the large-surface basal plane.

Although the lamellar structure is advantageous in terms of enhancing the volumetric capacitance, bare rGO-based electrodes exhibited a small capacitance of 20–30 F g^{-1}. This is because the electrolyte molecules cannot penetrate in between the close stacked graphene layers. The CNTs in the rPM[GO/oCNT] and r[GO-CNT] hybrid films, however, serve as physical spacers between the graphene layers for the insertion of electrolyte. Hence, the insertion of CNTs between the graphene layers leads to larger capacitance. We speculate that the difference in the specific capacitance between the rPM[GO/oCNT] and r[GO-CNT] resulted from the dispersion of CNTs in the layered graphene matrix. Chemical bonding between graphene and CNT may have prevented restacking of graphene layers and agglomeration of CNTs in solution, resulting in well-ordered lamellar structures. Furthermore, the chemically bonded CNTs in the composite film also bridge and seam the defects in the graphene edges and surface, facilitating electron transportation between graphene layers.[7,9,24]

Current research on supercapacitors aims to achieve the highest gravimetric capacitance. The theoretical maximum value of gravimetric capacitance of graphene is 550 F g^{-1}, as calculated from the intrinsic capacitance of single layer graphene as 21 μF cm^{-2}.[25] Researchers have focused on using graphitic porous materials with low density to achieve large gravimetric supercapacitors; however, the commercial drive is in the opposite direction with the major requirement being achieving large volumetric capacitances for the compact design of energy storage systems. Constructing high-density carbonaceous materials with optimum structure is the most critical criterion for producing high power and high energy supercapacitors.

Figure 4 shows the volumetric and gravimetric capacitances of different carbonaceous supercapacitor electrodes. The r[GO/CNT] material dealt with in this work showed improved volumetric capacitances and more dense electrodes in comparison

ADVANCED MATERIALS
www.advmat.de

www.MaterialsViews.com

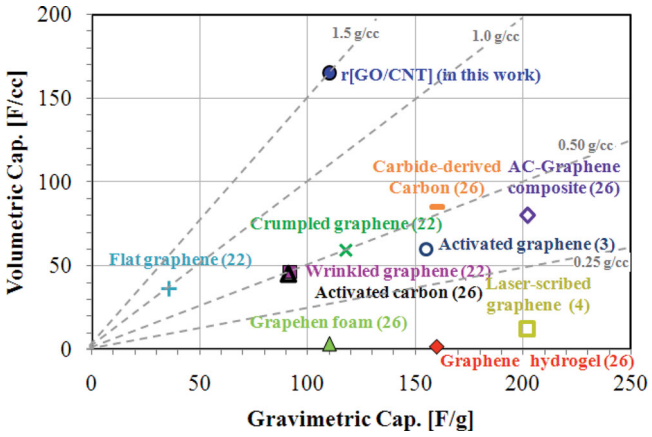

Figure 4. Comparison of the volumetric and gravimetric capacitances of r[GO/CNT] electrodes with other carbon electrodes. r[GO/CNT] exhibit a volumetric capacitance that is three-times larger than that of commercially available activated carbon-based supercapacitor electrode material. Data for other carbonaceous materials are adopted from various references.[3,4,22,26]

to other carbonaceous materials. For example, graphene foam and graphene hydrogel show high gravimetric capacitances of 110 and 160 F g^{-1}, respectively, albeit at very low densities of 0.01–0.03 g cm^{-3}, which result in small volumetric capacitances of 1–4 F cm^{-3}. Laser-scribed graphene also shows a very low density of 0.06 g cm^{-3} corresponding to a capacitance of 12.1 F g^{-1} because of the presence of large voids.

The controlled lamellar structure of graphene with chemically bonded CNT proposed in this work achieves a large volumetric capacitance corresponding to 160 F cm^{-3} with the high density electrode fabrication method used herein. It should be also noted that the density of this graphene composite is more than thrice that of activated carbon (0.4–0.5 g cm^{-3}), which is the dominant material used in EDLC electrodes. Hence, the material we propose in this work can be used practically in energy storage systems.

In conclusion, we have demonstrated a chemically linked graphene–CNT layered structure with controlled interlayer spacing. Because of the enlarged interlayer spacing ranging up to 0.55 nm, the r[GO/CNT] supercapacitor generated a volumetric capacitance of 165 F cm^{-3}, which is a performance much superior to other carbon based electrodes. Considering the needs of large volumetric capacitance, the use of these highly packed lamellar graphene/spacer structures may accelerate the development of new EDLC materials for the supercapacitor industry. Furthermore, this high-density graphene–CNT hybrid composite film may be also used for different applications such as electricity shielding or heat dissipation membranes.

Supporting Information

Supporting Information is available from the Wiley Online Library or from the author.

Received: June 19, 2013
Revised: July 30, 2013
Published online: September 19, 2013

[1] B. Xu, S. Yue, Z. Sui, X. Zhang, S. Hou, G. Cao, Y. Yang, *Energy Environ. Sci.* **2011**, *4*, 2826.
[2] a) L. L. Zhang, R. Zhou, X. S. Zhao, *J. Mater. Chem.* **2010**, *20*, 5983; b) A. Yu, I. Roes, A. Davies, Z. Chen, *Appl. Phys. Lett.* **2010**, *96*, 253105.
[3] a) Y. Zhu, S. Murali, M. D. Stoller, K. J. Ganesh, W. Cai, P. J. Ferreira, A. Pirkle, R. M. Wallace, K. A. Cychosz, M. Thommes, D. Su, E. A. Stach, R. S. Ruoff, *Science* **2011**, *332*, 1537; b) L. L. Zhang, X. Zhao, M. D. Stoller, Y. Zhu, H. Ji, S. Murali, Y. Wu, S. Perales, B. Clevenger, R. S. Ruoff, *Nano Lett.* **2012**, *12*, 1806.
[4] M. F. El-Kady, V. Strong, S. Dubin, R. B. Kaner, *Science* **2012**, *335*, 1326.
[5] a) M. F. El-Kady, R. B. Kaner, *Nat. Commun.* **2013**, *4*, 1475; b) Z. Niu, J. Chen, H. H. Hng, J. Ma, X. Chen, *Adv. Mater.* **2012**, *24*, 4144; c) Y. Xu, K. Sheng, C. Li, G. Shi, *ACS Nano* **2010**, *4*, 4324.
[6] Z.-D. Huang, B. Zhang, R. Liang, Q.-B. Zheng, S. W. Oh, X.-Y. Lin, N. Yousefi, J.-K. Kim, *Carbon* **2012**, *50*, 4239.
[7] X. Lu, H. Dou, B. Gao, C. Yuan, S. Yang, L. Hao, L. Shen, X. Zhang, *Electrochim. Acta* **2011**, *56*, 5115.
[8] a) H. R. Byon, S. W. Lee, S. Chen, P. T. Hammond, Y. Shao-Horn, *Carbon* **2011**, *49*, 457; b) D. Yu, L. Dai, *J. Phys. Chem. Lett.* **2009**, *1*, 467.
[9] Z.-D. Huang, B. Zhang, S.-W. Oh, Q.-B. Zheng, X.-Y. Lin, N. Yousefi, J.-K. Kim, *J. Mater. Chem.* **2012**, *22*, 3591.
[10] Y.-Y. Liang, L.-M. Zhang, *Biomacromolecules* **2007**, *8*, 1480.
[11] F. He, J. Fan, D. Ma, L. Zhang, C. Leung, H. L. Chan, *Carbon* **2010**, *48*, 3139.
[12] T. Ramanathan, F. T. Fisher, R. S. Ruoff, L. C. Brinson, *Chem. Mater.* **2005**, *17*, 1290.
[13] a) J. Zhu, J. Yang, B. Deng, *Environ. Chem. Lett.* **2010**, *8*, 277; b) J. An, J. Liu, Y. Zhou, H. Zhao, Y. Ma, M. Li, M. Yu, S. Li, *J. Phys. Chem. C* **2012**, *116*, 19699; c) J. Chen, M. A. Hamon, H. Hu, Y. Chen, A. M. Rao, P. C. Eklund, R. C. Haddon, *Science* **1998**, *282*, 95.
[14] Y. Zhou, Q. Bao, L. A. L. Tang, Y. Zhong, K. P. Loh, *Chem. Mater.* **2009**, *21*, 2950.
[15] a) Y. Si, E. T. Samulski, *Nano Lett.* **2008**, *8*, 1679; b) Y. Cao, J. Feng, P. Wu, *Carbon* **2010**, *48*, 1683.
[16] S. Stankovich, D. A. Dikin, R. D. Piner, K. A. Kohlhaas, A. Kleinhammes, Y. Jia, Y. Wu, S. T. Nguyen, R. S. Ruoff, *Carbon* **2007**, *45*, 1558.
[17] a) A. V. Murugan, T. Muraliganth, A. Manthiram, *Chem. Mater.* **2009**, *21*, 5004; b) H. M. A. Hassan, V. Abdelsayed, A. E. R. S. Khder, K. M. AbouZeid, J. Terner, M. S. El-Shall, S. I. Al-Resayes, A. A. El-Azhary, *J. Mater. Chem.* **2009**, *19*, 3832.
[18] D. Long, W. Li, L. Ling, J. Miyawaki, I. Mochida, S.-H. Yoon, *Langmuir* **2010**, *26*, 16096.
[19] R. Lv, Q. Li, A. R. Botello-Méndez, T. Hayashi, B. Wang, A. Berkdemir, Q. Hao, A. L. Elías, R. Cruz-Silva, H. R. Gutiérrez, Y. A. Kim, H. Muramatsu, J. Zhu, M. Endo, H. Terrones, J.-C. Charlier, M. Pan, M. Terrones, *Sci. Rep.* **2012**, 2.
[20] I. K. Moon, J. Lee, R. S. Ruoff, H. Lee, *Nat. Commun.* **2010**, *1*, 73.
[21] Y. Zhu, S. Murali, M. D. Stoller, A. Velamakanni, R. D. Piner, R. S. Ruoff, *Carbon* **2010**, *48*, 2118.
[22] J. Luo, H. D. Jang, J. Huang, *ACS Nano* **2013**, *7*, 1464.
[23] D. R. Dreyer, S. Park, C. W. Bielawski, R. S. Ruoff, *Chem. Soc. Rev.* **2010**, *39*, 228.
[24] B. G. Choi, M. Yang, W. H. Hong, J. W. Choi, Y. S. Huh, *ACS Nano* **2012**, *6*, 4020.
[25] J. Xia, F. Chen, J. Li, N. Tao, *Nat. Nanotechnol.* **2009**, *4*, 505.
[26] a) L. Zhang, F. Zhang, X. Yang, G. Long, Y. Wu, T. Zhang, K. Leng, Y. Huang, Y. Ma, A. Yu, Y. Chen, *Sci. Rep.* **2013**, 3; b) C. Largeot, C. Portet, J. Chmiola, P.-L. Taberna, Y. Gogotsi, P. Simon, *J. Am. Chem. Soc.* **2008**, *130*, 2730; c) Z. Niu, J. Chen, H. H. Hng, J. Ma, X. Chen, *Adv. Mater.* **2012**, *24*, 4143; d) M. A. Worsley, P. J. Pauzauskie, T. Y. Olson, J. Biener, J. H. Satcher, T. F. Baumann, *J. Am. Chem. Soc.* **2010**, *132*, 14067.